

PREDICTION OF WELD METAL MICROSTRUCTURE IN LASER BEAM WELDED CLAD STEEL

S. Missori¹ and A. Sili²

UDC 621.791.053.6:620.192

In dissimilar welded joints, data for the phase composition of the fusion zone may be taken from the phase equilibrium diagram composed in the course of experimental observation of phases. Results are given in the article for test laser welding of low-carbon steel plates, clad with austenitic stainless steel, and specimens are studied demonstrating perfection of the welded section austenitic microstructure. This confirms the data about the reliability of martensite-austenite boundaries studied by D. T. Kotecki on the example of chromium-nickel deposits prepared by submerged arc welding on carbon steel plates. Welds are studied by optical and scanning electron microscopy, and microhardness is determined by the Vickers method. The content of the main substitution alloying elements is calculated by means of energy-dispersion spectroscopy. The nitrogen content is determined using a hot gas extraction method and carbon is determined proceeding from the chemical composition of the deposited and base materials. It is established that the chromium and nickel content in points of the welded section with an entirely austenitic microstructure is specified by coordinates Cr_{eq} and Ni_{eq} in accordance with the austenite-martensite boundary proposed by Kotecki. Therefore, the results obtained confirm the possibility of predicting welded section microstructure from the position of this boundary, even in the case of joints welded with a laser beam with moderate solidification and cooling rates.

Keywords: clad steel, welding, laser beam, welded section, austenitic microstructure.

With the use of austenitic stainless steel filler metal for various welded joint materials (dissimilar or clad steels) during molten zone solidification there may be formation of numerous structures in relation to chemical composition, dilution of filler or basic metal, and cooling rate. Phase equilibrium diagrams in this case are a means of predicting the microstructure of stainless steels in relation to chemical composition: during many years since construction of the first Schaeffler and DeLong diagrams [1] numerous attempts have been made to study the process of phase formation in stainless steels. In particular, the authors in [2] have determined precise boundary lines for 100% ferrite and martensite by means of a metallographic method using selected etchants and colloidal suspensions of magnetic Fe_3O_4 particles. In addition, iso-ferrite lines and the boundary of austenite formation have been predicted qualitatively. With the aim of conformity for numerous results of magnetic measurements and special bending tests (ASME 2T bend tests), on the phase equilibrium diagram WRC-1992 (Welding Research Council) Kotecki has proposed a martensite-austenite boundary taking account of the effect of manganese content [3]. According to Kotecki, the upper boundary for martensite is not a line, but it may be determined as a narrow region between two parallel diagonal lines: above the upper line (austenite region) all bend tests were successful, whereas beneath the lower line (martensite region) all tests appeared to be unsuccessful. For chemical compositions within the limits of this region, the behavior during bending appeared to be uncertain, and the martensite content was unpredictable.

Recently, in order to predict the effect of temperature and alloying elements on welded joint phase formation, numerical thermodynamic methods are being considered [4]; in addition, several researchers have determined by experiment the

¹ Department of Industrial Engineering, University of Rome Tor Vergata, Rome, Italy; e-mail: missori@uniroma2.it.

² Department of Engineering, University of Messina, Messina, Italy; e-mail: asili@unime.it.

TABLE 1. Clad Steel Sheet Chemical Composition, wt.%

Metal	Thickness, mm	C	Mn	Si	P	S	Al	Cr	Ni	Mo	Fe
Base –ASTM A515 Gr.60	6.5	0.145	0.85	0.20	0.008	0.001	0.04	–	–	–	Balance
Cladding – AISI 304 L	2.5	0.017	1.32	0.39	0.029	0.003	–	18.39	10.07	–	Bal.

TABLE 2. Filler Metal Chemical Composition, wt.%

Metal	Form/sizes, mm	C	Mn	Si	Cr	Ni	Mo	Cu	Nb	Fe
<i>a</i> – NiCrMoCu32 28 7, DIN 1.4562 (specimen 1)	Wire/diam. 1.2	0.014	1.67	0.03	27.24	29.29	6.05	1.02	–	Bal.
<i>b</i> – AWS ER310 modified, DIN 1.4465 (specimen 2)	Strip/thickness 0.5	0.10	1.6	0.10	25.0	22.6	2.10	–	0.01	Bal.
<i>c</i> – AWS ER 308 DIN 1.4316 (specimen 3)	Wire/diam. 1.2	<0.025	1.7	<0.8	19.00	13.0	–	–	–	Bal.

microstructure of welded joints by x-ray diffraction and back-scattered electrons, [5], or by means of precise metallographic studies [6].

As is well known, in order to minimize joint metal hot cracking, mainly with an austenitic structure, it should have a small amount of δ -ferrite [7]. The amount of distribution of δ -ferrite depends to a considerable extent on chemical composition and cooling rate during metal solidification [8].

With a chemical composition similar to that of austenitic steel AISI 304, weld metal demonstrated different solidification modes. Its solidification as primary austenite is extremely undesirable: the probability of this solidification increases with an increase in Ni content, and also the solidification rate; solidification as primary δ -ferrite is due to a higher Cr content and slower solidification rate. Weld metal microstructure may either be entirely austenitic or contain a small amount of ferrite along grain and sub-grain boundaries (these solidification schemes are designated as A and AF, respectively). On the other hand, when solidification occurs with the formation of δ -ferrite, during cooling to room temperature a considerable part of it is transformed into austenite with some amount of residual ferrite (FA scheme) and the structure is less inclined towards crack formation. In contrast to ferrite, the presence of martensite in welded joint metal is undesirable, since it reduces ductility and facilitates cracking.

The possibility of fusion welding stainless and carbon steels, and numerous attempts at arc welding with a metal electrode in a protective gas atmosphere (GMAW) has shown that the formation of the accessible compounds for different steels is possible with appropriate combination of chemical composition of filler metal, welding rate, and current strength [9].

In previous research, the authors have attempted to obtain an FA-microstructure during welding different and clad steels. Sample multistage welding processes have been used combined with different procedures: welding with a single double laser beam (LBW) and also LBW + GMAW with different parameters and filler metals, which made it possible to obtain numerous weld metal specimens.

The microstructure of welded joints was studied by means of optical scanning electron microscopy (SEM), and Vickers microhardness was also studied. In order to calculate the equivalent chromium (Cr_{eq}) and nickel (Ni_{eq}) contents, the amount of substitution alloying elements was evaluated for the whole thickness of a welded joint by means of energy-dispersion spectroscopy (EDS method), nitrogen content was determined by means of a gas hot gas extraction method; carbon content was determined proceeding from the chemical composition of filler and basic metals.

In previous experiments, satisfactory joints have been obtained from the point of view of a lack of effects and final microstructure composition (i.e., austenite with a small amount of δ -ferrite without martensite) [10, 11]. In other specimens, the authors were unable to obtain the required chemical composition since the microstructure appeared to be entirely austenitic.

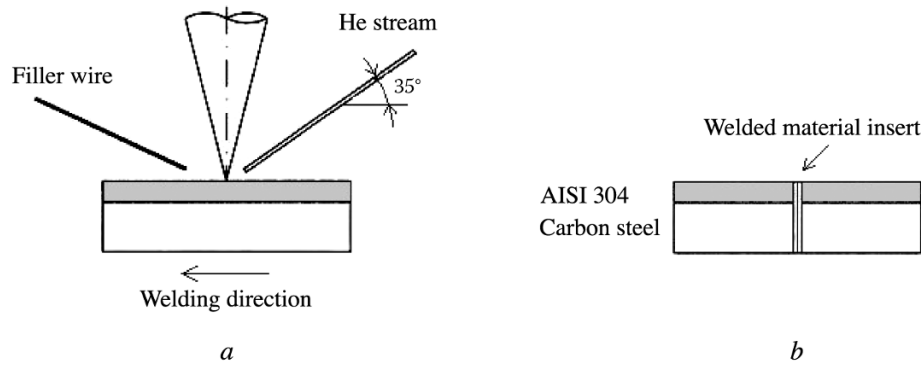


Fig. 1. Diagram of LBW process for clad steel: *a*) one-sided process with filler wire (specimen 1); *b*) cross section of working component with filler metal in the form of insert (specimen 2).

TABLE 3. Laser Beam Welding Process Parameters (specimens 1 and 2)*

Specimen	Power in welded component, kW	Welding rate v , m/min	Heat input H , kJ/m
1	10	2.0	300
2	10	1.6	375

* Sheet in a horizontal plane, laser beam movement over horizontal axis (Fig. 1).

TABLE 4. Parameters of Combined Laser Beam and Arc Welding with a Metal Electrode in a Protective Gas Atmosphere (specimen 3)*

Parameter	Value
<i>Arc welding in a protective gas atmosphere</i>	
Voltage, V	38.2
Current, A	472
Filler wire supply rate, m/min	15
Welding rate, m/min	1.2
Filler wire 1.2 mm in diameter chemical composition, see Table 2	Type <i>c</i>
Protective gas – argon, consumption (liters/min)	15
<i>Laser beam welding</i>	
Power in welded component, kW	5.0
Protective gas – helium, consumption (liters/min)	30
Distance between sections made by arc and laser welding, mm	55

* Sheet arranged in horizontal plane, laser beam movement over horizontal axis, see Fig. 2.

In this work, specimens have been studied with an austenitic microstructure, i.e., with the aim of checking the reliability of martensite-austenite boundaries, studied by Kotecki on the example of single-pass chromium-nickel fillers of stainless steel, performed by submerged-arc welding in plates of stainless steel.

Materials. Clad plates, prepared from low-carbon steel (thickness 6.5 mm) by hot rolling with austenitic stainless steel (thickness 2.5 mm) were welded in one pass by a laser beam simple or combined), and also arc welding the chemical composition of the plates of clad steels is given in Table 1. The filler meal was used in the form of wire strip (Table 2). Welded plates were neither previously heated nor given post-welding heat treatment.

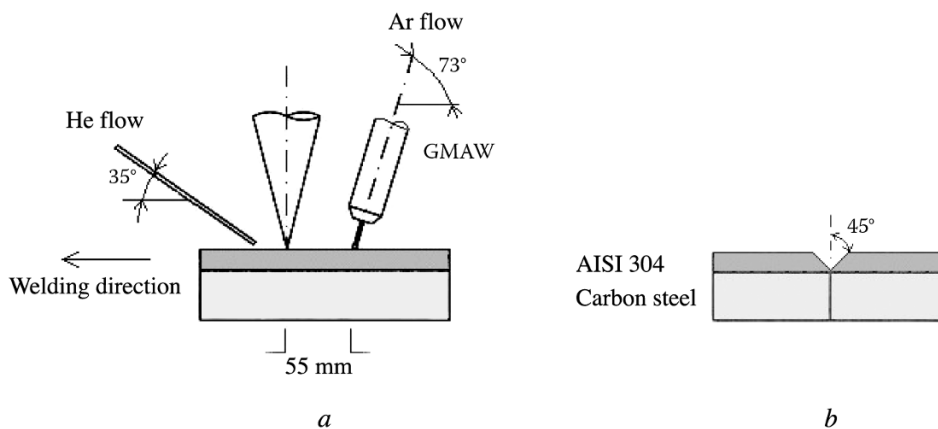


Fig. 2. Welding by LBW and GMAW processes (specimen 3): *a*) layout of combined process; *b*) workpiece section with separating groove.

Laser beam welding (LBW). Welding of two different specimens was performed in a flat position (Fig. 1a) using one laser beam from the direction of the clad steel. Welded plates had uniform edges (without bevelling).

Two filler metals were used: for specimen 1 it was wire (diameter 1.2 mm) of alloy *a*; for specimen 2 it was two strips (each 0.5 mm thick) of alloy *b* (see Table 2). Before welding, both strips of filler metal were arranged between the flat edges of plates (Fig. 1b). Welding process parameters are given in Table 3. Protection of the weld bath and control of the plasma was accomplished by a stream of helium gas (flow rate 20–25 liters/min).

Combined LBW and GMAW welding process. For clad plates, there was a successive combination of welding processes by a laser beam (LBW) and arc welding with a metal electrode in a protective gas atmosphere (GMAW). Two welding baths and two individual plasma controllers were used for welding of both forms with a distance of 55 mm between the corresponding points of action: first a laser beam and then an arc. There were two streams of protective gas: helium for laser welding and argon for arc welding with metal electrodes (Fig. 2). Process parameters are provided in Table 4.

We used this combined process in practice in order to employ the possibility of deep penetration of a laser beam and to achieve increased tolerance for geometric defects during arc welding. Finishing of sheet edges for welding was accomplished by means of a V-shaped section trough, and welding was performed in the lower position with the clad side of a specimen with a laser beam and a flame. Filler material was in the form of wire (diameter 1.2 mm), see type *c*, Table 2.

Experiment description. After visual and macrographic examination of a joint, it was cut across the deposited metal in order to obtain specimens of welded joint cross section. The microstructure of the weld zone (WZ) and heat-affected zone (HAZ) was studied in metallographic specimens prepared by traditional mechanical polishing and etching with Vilella's reagent.

The content of the main substitutional elements was determined by means of EDS microanalysis over the edge at ten points located along the central line of a welded joint, with intersection of the whole specimen thickness (volume of material reacting with electron beam during each measurement is several cubic microns).

The welded joint nitrogen content was measured by the procedure of hot gas extraction using a LECO TC400 N/O instrument: specimen volume about 100 mm³, cut from a welded zone, melted in a graphite crucible, and the gas obtained was analyzed by means of a sensitive thermal conduction cell. This test guarantees stable measurement of the nitrogen concentration independent of discharge of gas and a wide pressure range, but the volume of material analyzed in this case is an order of magnitude greater than during EDS microanalysis. Therefore, these measurements should be considered as determination of the average nitrogen content in welded joints.

The carbon content was calculated proceeding for the composition of the basic and filler metals taking account of their actual contribution in forming a WZ in view of dilution on the basis of measured values of the melted zone area. These values were calculated from measurement of the melted zone profile, separated into layers of identical thickness, performed in an optical microscope.

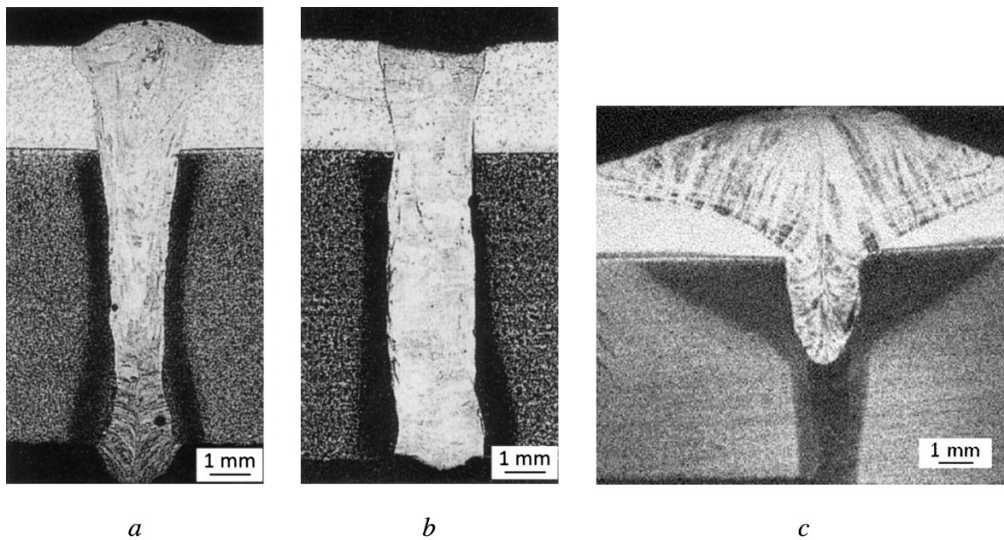


Fig. 3. Welded joint section: *a, b*) LBW welding (*a* is specimen 1; *b* is specimen 2); *c*) after combined LBW and GMAW welding (specimen 3).

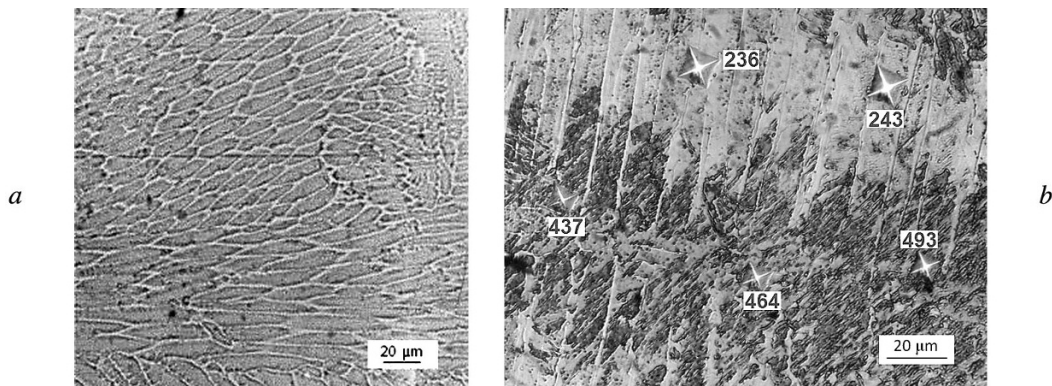


Fig. 4. Structure of entirely austenitic zone (*a*) and mixed martensite-austenite zone with Vickers microhardness indicated (*b*).

Attention is drawn to the martensite-austenite boundary suggested by Kotecki for $[Mn] = 1\%$ [3], and therefore that in these experiments the manganese content appeared to be much lower than 1%. The composition of welded joints was expressed in terms of Cr_{eq} and Ni_{eq} (%) in accordance with the following relationships and used for WRC-1992 composition diagram [3]:

$$Cr_{eq} = Cr + Mo + 0.7Nb, \quad Ni_{eq} = Ni + 35C + 20H + 0.25Cu. \quad (1)$$

Vickers microhardness (load 100 g) was determined in a transverse line of metallographic specimens along the axis of the WZ line and also in transverse lines parallel to cladding lines correspondingly in the center of the thickness of the cladding thickness and within the center of the thickness of the carbon steel base. A smaller load (25 g) was used locally for the more precise determination of martensite and austenite in the case of mixed microstructures.

Results and discussion. The cross sections of joints of clad steel prepared by the LBW method are narrower than those obtained with a combine process (Fig. 3). All joints had satisfactory external appearance with visual and macrographic

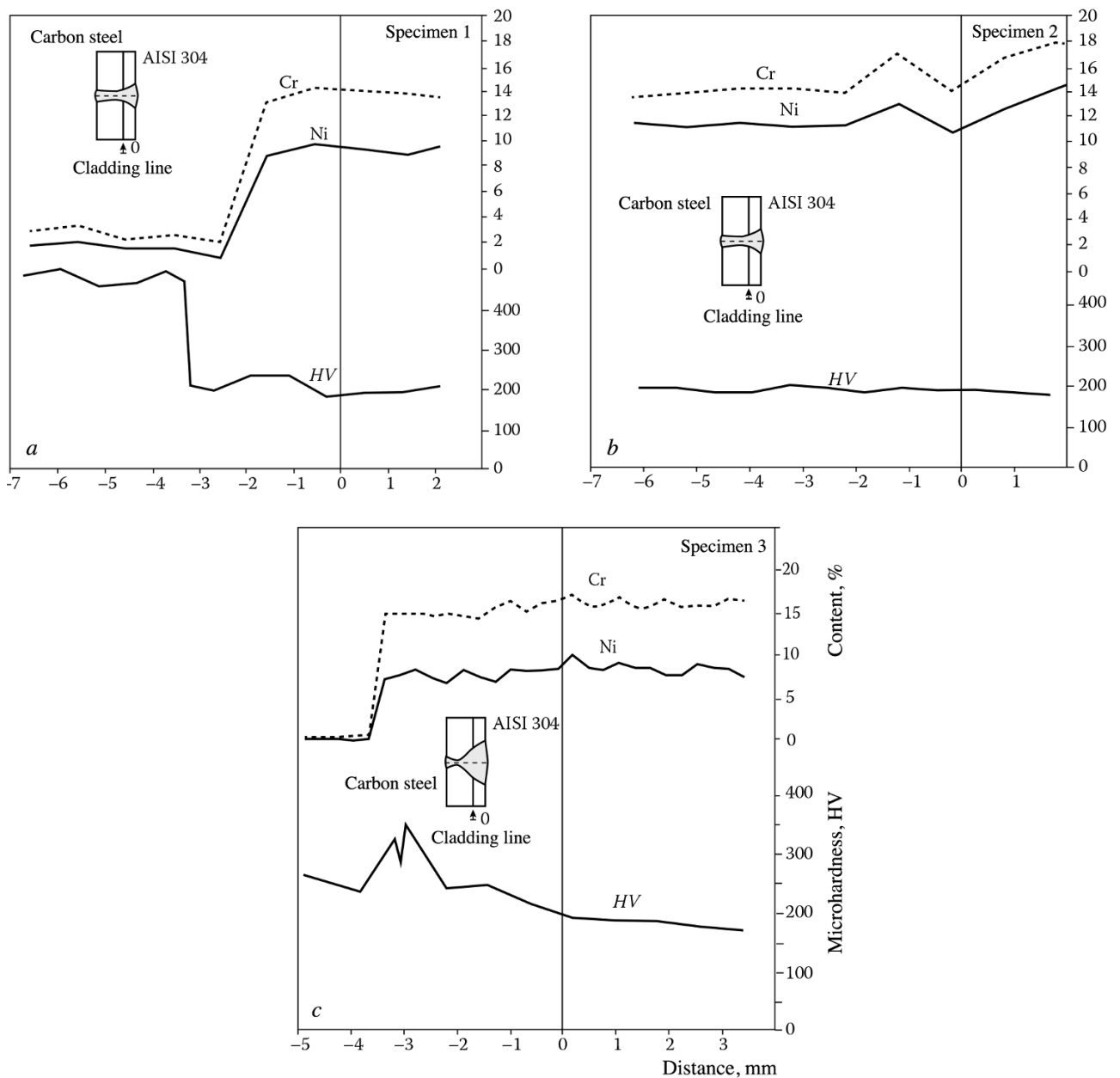


Fig. 5. Results of EDS measurements (energy dispersion spectrometry) and microhardness measurement over whole thickness for specimens 1 (a), 2 (b), and 3 (c).

examination. With the exception of some small slight porosity, there was no marked inhomogeneity (cracks and incomplete fusion) in welded joints.

A microstructure is shown in Fig. 4a of an entirely austenitic zone. For comparison, a martensite-austenite structure is shown (Fig. 4b): results of microhardness measurement (with a 25-g load) make it possible to distinguish both phases.

Specimen 1 prepared with a one-sided LBW process with filler wire has a sharp reduction in content of the main alloying elements (Cr and Ni) through its thickness from the layer of the AISI 304 metal to the layer of carbon steel (Fig. 5a).

The presence of austenite was detected metallographically in the clad side and martensite was seen in the carbon steel side according to microhardness distribution through a whole specimen thickness: about 180–200 HV from the direction of the clad steel to a value of the order of 450 HV in the carbon steel side.

TABLE 5. Position of Experimental Points and Main Elements' Content

Specimen number	Point number	Distance, μm	Element content, wt.%					
			Cr	Ni	Mn	Mo	C	N
1	1.1	-300	14.2	9.9	1.1	0.7	0.08	0.05
	1.2	500	14.1	9.5	1.2	0.7	0.08	0.05
	1.3	1300	13.8	9.0	1.2	0.7	0.08	0.05
	1.4	2100	13.5	9.6	1.3	0.7	0.08	0.05
2	2.1	-6050	13.4	11.4	1.2	1.2	0.03	0.05
	2.2	-5350	13.7	11.0	1.2	1.2	0.03	0.05
	2.3	-1850	13.8	11.3	1.3	1.2	0.03	0.05
	2.4	-450	13.9	10.7	1.3	1.2	0.03	0.05
3	3.1	1000	15.9	8.4	1.3	0.2	0.04	0.04
	3.2	1800	15.6	8.7	1.4	0.4	0.04	0.04
	3.3	2500	15.9	9.1	1.4	0.3	0.04	0.04

TABLE 6. Values of Ni_{eq} , Cr_{eq} (wt.%), and Vickers Microhardness

Specimen number	Point number	Distance, μm	Cr_{eq} , %	Ni_{eq} , %	Hardness, HV (100 g – 10 sec)
1	1.1	-300	14.9	13.7	181
	1.2	500	14.8	13.3	188
	1.3	1300	14.5	12.8	193
	1.4	2100	14.2	13.4	203
2	2.1	-6050	14.6	13.5	195
	2.2	-5350	14.9	13.1	195
	2.3	-1850	15.0	13.5	184
	2.4	-450	15.1	12.8	192
3	3.1	1000	16.1	10.4	187
	3.2	1800	16.0	10.7	187
	3.3	2500	16.2	11.1	177

In specimen 2, due to uniform contribution of filler metal strips, the Cr and Ni content is quite uniformly distributed through the whole of the thickness (Fig. 5b). The microstructure observed is entirely austenitic throughout the whole specimen thickness and with quite uniform microhardness (180–200 HV).

In specimen 3 welded by the combined LBW + GMAW processes, the clad side was highly alloyed, whereas on the opposite side the Cr and Ni contents were zero (see Fig. 5c).

In the carbon steel side at a distance from the cladding line, the microstructure is martensitic with a maximum microhardness value up to about 300–350 HV. In the clad steel side, the microstructure is austenitic, and microhardness is in the range 180–190 HV.

Results of an experiment for eleven points selected in the austenitic region of welded joints are given in Table 5. Welded joints are highly alloyed with Cr and Ni, but the Mn content is slightly greater than 1%, and the Mo content is in the range 0.3–0.7%.

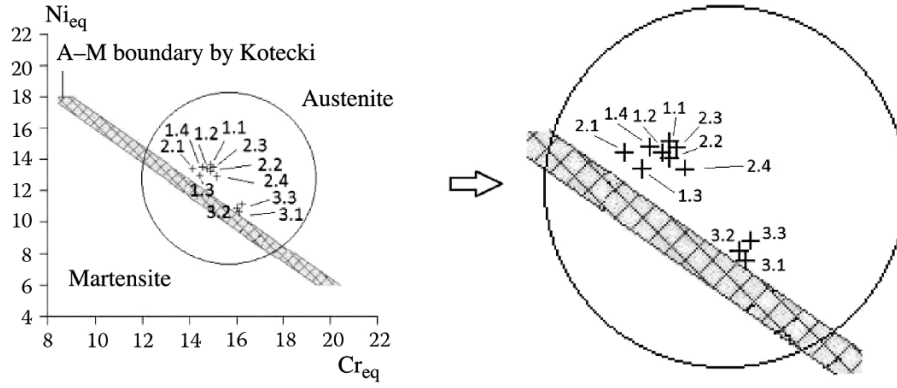


Fig. 6. WRC-1992 constitution diagram with martensite-austenite boundary proposed by Kotecki for [Mn] = 1% [3], and position of 11 experimental points.

Values of Ni_{eq} and Cr_{eq} calculated by Eq. (1) and the results of microhardness measurements and the microstructure observed are given in Table 6. An austenitic microstructure is obtained at all points.

Since the microstructure at all these points is austenitic, they fall in the austenitic region of the WRC-1992 composition diagram (Fig. 6), but outside the limits proposed by Kotecki for deposited weld joint metal containing Mn = 1% [3].

It should be noted that the LBW process may give rise to a faster welded joint metal cooling rate than traditional arc melting processes. This may cause a change in the behavior of metal during solidification and consequently deviation from the microstructures desired [12].

The authors of the present work evaluated the solidification time and cooling rate after solidification with the aim of confirming the fact that in this case the cooling rate is relatively moderate compared with other LBW process conditions with extremely reduced size of the fusion zone and low values of heat input. The evaluation is based on well-known relationships [13]. The solidification time t_s is determined from an expression

$$t_s = LH_{net} / (2\pi k \rho C (T_m - T_0)^2). \quad (2)$$

Data for approximate determination of t_s for specimen 2:

$$L \text{ (latent heat of solidification)} = 2 \cdot 10^9 \text{ J/m}^3;$$

$$T_m \text{ (steel melting temperature)} = 1460^\circ\text{C};$$

$$T_0 \text{ (room temperature)} = 20^\circ\text{C};$$

$$\nu \text{ (welding rate)} = 1.6 \text{ m/min};$$

$$W \text{ (net welding power)} = 10000 \text{ W};$$

$$\eta \text{ (LBW process efficiency)} = 0.8;$$

$$H_{net} \text{ (net heat input)} = \eta W / \nu = 0.8 \cdot 10000 \cdot 60 / 1.6 = 3 \cdot 10^5 \text{ J/m};$$

$$k \text{ (austenitic steel specific thermal conductivity)} = 12 \text{ W/(m}\cdot^\circ\text{C)};$$

$$\rho C \text{ (austenitic steel heat capacity)} = 7990 \cdot 0.50 = 4 \cdot 10^6 \text{ J/(}^\circ\text{C}\cdot\text{m}^3\text{)}.$$

Then, $t_s \approx 0.96$ sec and solidification rate R_s (considering a solidification interval of 30 sec) is determined as

$$R_s = \Delta T / t_s = 30 / 0.96 \approx 31^\circ\text{C/sec}. \quad (3)$$

The maximum cooling rate after solidification R is estimated by the relationship

$$R = 2\pi k \rho C (s / H_{net})^2 (T_c - T_0)^3. \quad (4)$$

Assuming the cooling rate R is a maximum at temperature $T_c = 1420^\circ\text{C}$ (a little lower than the crystallization point) for plates with $s = 0.009$ m, we obtain $R \approx 745$ °C/sec.

Therefore, the solidification time and cooling rate with laser beam welding correspond to the same values as with normal arc welding processes.

The microstructures observed were formed under conditions comparable to those of traditional arc welding processes; therefore, the expediency of predicting phases based on the WRC-1992 diagram appears to be reasonable.

Conclusion. Several joints of low-carbon steel plates clad with austenitic steel, accomplished by a LBW process or combined LBW and GMAW processes with moderate values of solidification time and cooling rate were studied by means of SEM microanalysis, hot gas extraction analysis, metallographic examination, and microhardness measurement. The calculated values of Cr_{eq} and Ni_{eq} for several experimental points, selected with an entirely austenitic structure, were represented in the WRC 1992 diagram. They agree with this diagram, falling within the austenitic region above the austenite-martensite boundary proposed by Kotecki for a content of $\text{Mn} = 1\%$. Therefore, our experiments have shown that this boundary is valid even in the case when compounds made with a laser beam solidify and are cooled at rates comparable with typical rates for traditional arc welding processes.

The authors thank the Fraunhofer Institut für Lasertechnik (ILT), Aachen (Germany) for providing assistance in performing welding trials in their laboratories.

REFERENCES

1. G. Krauss, *Steel: Processing, Structure, and Performance*, ASM International, Metals Park (2005), 2nd ed.
2. M. C. Balmforth and J. C. Lippold, "A new ferritic-martensitic stainless steel constitution diagram," *Welding J.*, **79**, No. 12, 340–345 (2000).
3. D. J. Kotecki, "A martensite boundary on the WRC-1992 diagram: the effect of manganese," *Welding J.*, **79**, No. 12, 346–354 (2000).
4. S. Wessman, "Evaluation of the WRC 1992 diagram using computational thermodynamics," *Welding in the World*, **57**, No. 3, 305–313 (2013).
5. A. Eghlimi, M. Shamanian, M. Eskandarian, et al., "Evaluation of microstructure and texture across the welded interface of super duplex stainless steel and high strength low alloy steel," *Surf. Coat. Technol.*, **264**, 150–162 (2015).
6. H. Tasalloti, P. Kah, and J. Martikainen, "Effect of heat input on dissimilar welds of ultra high strength steel and duplex stainless steel: microstructural and compositional analysis," *Mater. Characteriz.*, **123**, 29–41 (2017).
7. J. Lippold, *Welding Metallurgy and Weldability*, John Wiley & Sons, New Jersey (2015).
8. A. F. Padilha, C. Fazzioli Tavares, and M. A. Martorano, "Delta ferrite formation in austenitic stainless steel castings," *Mater. Sci. Forum*, **730–732**, 733–738 (2013).
9. B. Mvola, P. Kah, and J. Martikainen, "Dissimilar ferrous metal using advanced gas metal arc welding processes," *Rev. Adv. Mater. Sci.*, **38**, 125–137 (2014).
10. S. Missori, F. Murdolo, and A. Sili, "Single-pass laser beam welding of clad steel plate," *Welding J.*, **83**, No. 2, 65–71 (2004).
11. S. Missori, A. Sili, and N. Ucciardello, "Process parameters optimization of laser beam welded joints by neural network," *Mater. Manufact. Proc.*, **23**, No. 2, 168–173 (2008).
12. V. Kujanpää, "Thick-section laser and hybrid welding of austenitic stainless steels (8th Int. Conf. on Photonic Technologies LANE 2014)," *Phys. Procedia*, **56**, 630–636 (2014).
13. *Welding Handbook*, American Welding Society, Miami (2002), Vol. 1, 9th ed.